PHYSICAL REVIEW B **76**, 201401(R) (2007)

Probing the electronic structure of bilayer graphene by Raman scattering

L. M. Malard,[1] J. Nilsson,[2] D. C. Elias,[1] J. C. Brant,[1] F. Plentz,[1] E. S. Alves,[1] A. H. Castro Neto,[2] and M. A. Pimenta[1]
[1]*Departamento de Física, Universidade Federal de Minas Gerais, 30123-970 Belo Horizonte, Brazil*
[2]*Department of Physics, Boston University, 590 Commonwealth Avenue, Boston, Massachusetts 02215, USA*
(Received 14 September 2007; published 1 November 2007)

The electronic structure of bilayer graphene is investigated from a resonant Raman study of the G' band using different laser excitation energies. The values of the parameters of the Slonczewski-Weiss-McClure model for bilayer graphene are obtained from the analysis of the dispersive behavior of the Raman features, and reveal the difference of the effective masses of electrons and holes. The splitting of the two TO phonon branches in bilayer graphene is also obtained from the experimental data. Our results have implications for bilayer graphene electronic devices.

DOI: 10.1103/PhysRevB.76.201401 PACS number(s): 73.21.−b, 63.20.Kr, 78.30.−j, 81.05.Uw

Differently from monolayer graphene, where the electrons behave like *massless* Dirac fermions and exhibit a linear dispersion near the Dirac point, the electrons in bilayer graphene are described by nonzero effective mass Dirac fermions with a parabolic electronic dispersion.[1] Furthermore, while the unbiased bilayer graphene is a zero-gap semiconductor, a biased bilayer is a tunable gap semiconductor by electric field effect.[2,3] Hence the development of bilayer graphene-based bulk devices depends on the detailed understanding of its electronic properties. This work shows that, by performing Raman scattering experiments in bilayer graphene with many different laser excitation energies, we can probe its electronic structure and we can obtain experimental values for the Slonczewski-Weiss-McClure (SWM) parameters[4,5] for bilayer graphene.

Figure 1 shows the atomic structure of a bilayer graphene, in which we can distinguish the two nonequivalent atoms A and B in each plane giving rise to a unit cell with four atoms. Since this unit cell is the same for graphite in the Bernal stacking structure, we can describe the electronic spectrum of bilayer graphene in terms of the SWM model for graphite,[4,5] by determining the parameters γ_0, γ_1, γ_3, and γ_4, that are associated with overlap and transfer integrals calculated for nearest neighbor atoms. The pair of atoms associated with these parameters is indicated in the atomic structure of a bilayer graphene shown in Fig. 1(a). These parameters, that are fundamental for the electronic processes in the system, are only roughly known to this date.

The graphene samples used is this experiment were obtained by a micromechanical cleavage of graphite on the surface of a Si sample with a 300 nm layer of SiO_2 on the top.[1] The bilayer flakes were identified by the slight color change from monolayer graphene in an optical microscope, followed by a Raman spectroscopy characterization using the procedure described by Ferrari *et al.*[6] For the Raman measurements, we used a Dilor *XY* triple monochromator in the backscattering configuration. The spot size of the laser was ~ 1 μm using a 100× objective and the laser power was kept at 1.2 mW in order to avoid sample heating. Raman spectra were obtained for 11 different laser lines of Ar-Kr and dye lasers in the range 1.91–2.71 eV.

Recently, Ferrari *et al.*[6] showed that Raman spectroscopy can be used to identify the number of layers in a graphene sample and, in particular, to clearly distinguish a monolayer from a bilayer graphene sample. Figure 2 shows the Raman spectra of the monolayer [Fig. 2(a)] and bilayer [Fig. 2(b)] graphene samples, where the most prominent features are the G and G' Raman bands.[7]

The G' band of the monolayer graphene can be fitted by just one Lorentzian with a full width at half maximum (FWHM) of 24 cm^{-1}. A better adjustment can be obtained with Voigt functions, which have four fitting parameters. However, different sets of four Voigt parameters fit the G' band equally well, preventing a precise physical interpretation of these parameters. Therefore we decided to analyze the data using the Lorentzian functions. The G' band for bilayer graphene was fitted using four Lorentzian peaks, all of them having the same FWHM of 24 cm^{-1} used to fit the G' band of monolayer graphene, in agreement with the previous Raman studies of graphene systems.[6,8,9] The relative amplitudes of the four Lorentzians depend on the laser energy; two of them increase and the other two decrease with increasing laser energy. The fit was done by following the trend of the laser energy dependence of these relative intensities.

The Raman spectra of both the monolayer and bilayer graphene have been measured with many different laser energies in the visible range. Figure 3 shows the laser energy dependence of the G'-band frequency for the monolayer sample [Fig. 3(a)] and for each one of the four peaks that comprise the G' band for bilayer graphene [Fig. 3(b)].

The origin of the G' band in all graphitic materials is due to an intervalley double-resonance (DR) Raman process[10,11]

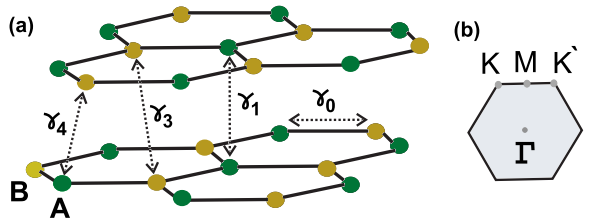

FIG. 1. (Color online) (a) Atomic structure of bilayer graphene. The A atoms of the two layers are over each other, whereas the B atoms of the two layers are displaced with respect to each other. The SWM constants γ_0, γ_1, γ_3, and γ_4 label the corresponding pair of atoms associated with the hopping processes. (b) First Brillouin zone of monolayer graphene, showing the high symmetry points Γ, K, K', and M.

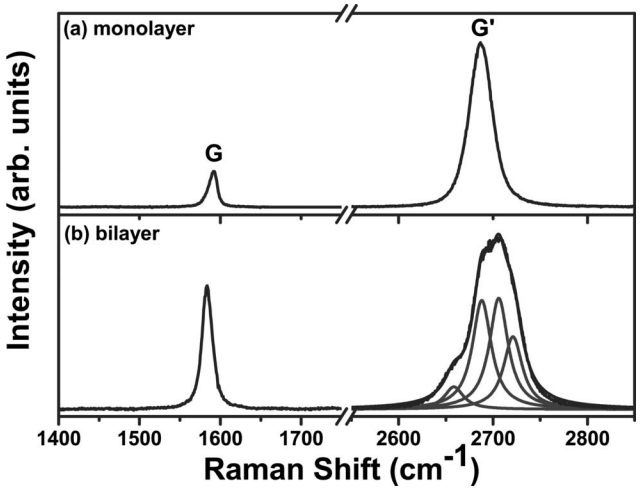

FIG. 2. (a) Raman spectrum of the monolayer graphene and (b) Raman spectrum of the bilayer graphene performed with the 2.41 eV laser line.

involving electronic states near two nonequivalent K points (K and K') in the first Brillouin zone of graphene [see Fig. 1(b)], and two phonons of the iTO branch.[7,12] As a result of the angular dependence of the electron-phonon matrix elements[13] and the existence of interference effects in the Raman cross section,[12] the main contribution for the G' band comes from the particular DR process that occurs along the Γ-K-M-K'-Γ direction, in which the wave vectors k and k' of the two intermediate electronic states in the conduction band (measured from the K and K' points, respectively) are along the $K\Gamma$ and $K'\Gamma$ directions, respectively.[6] Therefore the wave vector q of the phonons involved in this specific process is along the KM direction and is related to the electron wave vectors by the condition $q=k+k'$.[7]

In the case of the bilayer graphene, where the two graphene layers are stacked in a Bernal configuration,[7] the π-electrons dispersion in the valence and in the conduction

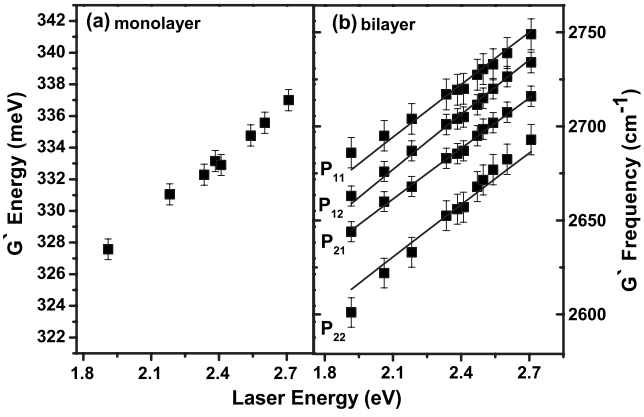

FIG. 3. (a) Laser energy dependence of the G'-band energy for a monolayer graphene. (b) Laser energy dependence of the positions of the four peaks that comprise the G' band of bilayer graphene. These four Raman peaks originate from the P_{11}, P_{12}, P_{21}, and P_{22} DR processes illustrated in Fig. 4. The black squares are the experimental data and the full lines are the fitted curves (see discussion in the text).

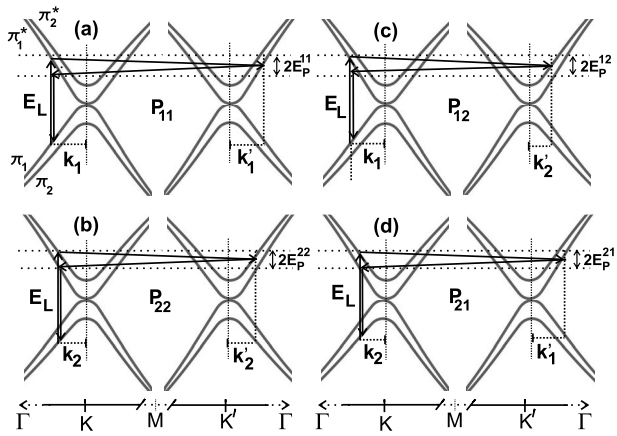

FIG. 4. Schematic view of the electron dispersion of bilayer graphene near the K and K' points showing both π_1 and π_2 bands. The four DR processes are indicated: (a) process P_{11}, (b) process P_{22}, (c) process P_{12}, and (d) process P_{21}. The wave vectors of the electrons (k_1, k_2, k_1', and k_2') involved in each of these four DR processes are also indicated.

band splits into two parabolic branches near the K point,[14] as shown in Fig. 4. In this figure, the upper and lower branches of the valence band are labeled as π_1 and π_2, respectively. The lower and upper branches of the conduction band are called π_1^* and π_2^*, respectively. Along the high symmetry Γ-K-M-K'-Γ direction, these branches belong to different irreducible representations of the $P6_3/mmc$ space group and therefore only the $\pi_1 \rightleftarrows \pi_1^*$ and $\pi_2 \rightleftarrows \pi_2^*$ optical transitions between the valence and conduction bands are allowed. Therefore there are four possible intervalley DR processes involving electrons along the Γ-K-M-K'-Γ direction that lead to the observation of the four peaks of the G' band of bilayer graphene.[6]

The four DR processes are represented in Fig. 4. In process P_{11} [Fig. 4(a)], an electron with wave vector k_1 is resonantly excited from the valence band π_1 to the conduction band π_1^* by absorbing a photon with energy E_L. This electron is then resonantly scattered to a state with wave vector k_1' by emitting a phonon with momentum q_{11} and energy E_p^{11}. Finally, the electron is scattered back to state k_1 by emitting a second phonon, and it recombines with a hole producing a scattered photon with an energy $E_S=E_L-2E_p^{11}$. The phonon wave vector q_{11}, measured from the K point and along the KM direction, is given by $q_{11}=k_1+k_1'$.

Figure 4(b) shows the DR process P_{22}, which involves an electron that is optically excited between the π_2 and π_2^* branches. The energy of the associated phonon is E_p^{22} and its wave vector is given by $q_{22}=k_2+k_2'$. Figures 4(c) and 4(d) show processes P_{12} and P_{21} that involve electrons with wave vectors k_1, k_2' and k_2, k_1', respectively, which belong to different electron branches. The wave vectors of the phonons associated with processes P_{12} and P_{21} are given by $q_{12}=k_1+k_2'$ and $q_{21}=k_2+k_1'$, respectively.

The two iTO phonon branches of a bilayer graphene along the ΓKM line belong to the irreducible representations T_1 and T_3. The scattering of an electron in the conduction band between states around K and K' has to satisfy the electron-phonon selection rule, so that the allowed transi-

tions are $\pi_1^* \rightleftarrows \pi_1^*$ or $\pi_2^* \rightleftarrows \pi_2^*$ for the T_1 phonon and $\pi_2^* \rightleftarrows \pi_1^*$ for the T_3 phonon. Since processes P_{11} and P_{22} involve electrons states around K and K' which belong to the same electronic branch, the associated phonons belong to the T_1 phonon branch. On the other hand, phonons involved in processes P_{12} and P_{21} belong to the T_3 branch.

From Fig. 4 one can see that the phonon associated with the P_{11} process has the largest wave vector (q_{11}). Since the energy of the iTO phonon increases with increasing q, the highest frequency component of the G' band of a bilayer graphene is related to the P_{11} process. On the other hand, P_{22} process is associated with the smallest phonon wave vector q_{22}, and gives rise to the lowest frequency component of the G' band of a bilayer graphene. The two intermediate peaks of the G' band are associated with processes P_{12} and P_{21}.

In order to analyze the experimental results shown in Fig. 3(b), we must find a relation between the electronic and the phonon dispersions of a bilayer graphene, according to the DR Raman process. The electronic dispersion of the bilayer graphene can be described in terms of the standard SWM model for graphite [see, e.g., Eq. (2.1) in Ref. 4] and using the full tight-binding dispersion introduced originally by Wallace.[15] Along the K-Γ direction this amounts to replacing σ by $\gamma_0[2\cos(2\pi/3 - ka\sqrt{3}/2)+1]$ in McClure's expressions. Here k is measured from the K point and $a=1.42$ Å is the in plane nearest neighbor carbon distance. Since there is no k_z dependence we may set $\Gamma=1$ and $\gamma_2=\gamma_5=0$ (γ_2 and γ_5 correspond to third layer interactions in graphite). We have verified that the parameter Δ does not make any noticeable difference in our results and will be ignored in our analysis. With these simplifications, the bands in the bilayer are parametrized by the four parameters γ_0, γ_1, γ_3, and γ_4. A more detailed account of this approach to the band structure calculation of the graphene bilayer can be found in Ref. 16.

In fact, along the high symmetry K-Γ direction, the 4×4 matrix factorizes and the dispersion of the four bands are given by

$$E_{\pi_2} = (-\gamma_1 - v_3\sigma - \xi_+)/2, \tag{1a}$$

$$E_{\pi_1} = (\gamma_1 + v_3\sigma - \xi_-)/2, \tag{1b}$$

$$E_{\pi_1^*} = (-\gamma_1 - v_3\sigma + \xi_+)/2, \tag{1c}$$

$$E_{\pi_2^*} = (\gamma_1 + v_3\sigma + \xi_-)/2, \tag{1d}$$

where

$$\xi_\pm = \sqrt{(\gamma_1 - v_3\sigma)^2 + 4(1 \pm v_4)^2\sigma^2}, \tag{2}$$

and $v_j \equiv \gamma_j/\gamma_0$.

In order to obtain the dependence of the phonon energy E_p^{ij} on the laser energy E_L, let us consider a generic process P_{ij}, where i, $j=1$ or 2, which describes the four processes shown in Fig. 4. In the first step of this process (electron-hole creation), the incident photon is in resonance with the electronic states in the valence and conduction bands at the k_i point. Thus the laser energy E_L can be written as

TABLE I. Values obtained for the phonon dispersion of the two iTO phonon branches of bilayer graphene near the K point, where $E_p^{ii}=A_{ii}+B_{ii}q$ corresponds to the P_{11} and P_{22} processes and $E_p^{ij}=A_{ij}+B_{ij}q$ to the P_{12} and P_{21} processes.

A_{ii}	B_{ii}	A_{ij}	B_{ij}
153.7 (meV)	38.5 (meVÅ)	154.0 (meV)	38.8 (meVÅ)
1238 (cm^{-1})	310 (cm^{-1} Å)	1241 (cm^{-1})	313 (cm^{-1} Å)

$$E_L = E_{\pi_i^*}(k_i) - E_{\pi_i}(k_i). \tag{3}$$

Equation (3) allows us to determine the momentum k_i of the electron excited in the process.

The electron is then resonantly scattered from the vicinity of the K point to the vicinity of the K' point by emitting a (iTO) phonon with energy E_p^{ij} given by

$$E_p^{ij}(k_i + k_j') = E_{\pi_i^*}(k_i) - E_{\pi_j^*}(k_j'). \tag{4}$$

Assuming that we know the iTO phonon dispersion near the K point $[A+B(k_i+k_j')]$ as well as the bands involved [Eqs. (1) and (2)] Eq. (4) uniquely determines the momentum of the scattered electron k_j'. We then compute the phonon energy E_p^{ij}, that is directly related to the Raman shift for this specific P_{ij} process, obtained with a given laser energy E_L. Finally, we perform a least-squares fit to determine the parameters γ_0, γ_1, γ_3, and γ_4 of the model [Eqs. (1) and (2)] that give the best fit of the dispersion of the four G' peaks in bilayer graphene shown in Fig. 3. The four solid lines in Fig. 3(b) represent the best fitting of the experimental E_p^{ij} vs E_L data.

We have also tried to fit, unsuccessfully, our experimental data for the four DR processes taking only γ_0, γ_1, and γ_3. Therefore in order to get a good fitting, the parameter γ_4, which is associated with the splitting of the two G' intermediate peaks, has to be included. For the dispersion of the iTO phonon branches near the K point, we could not fit satisfactorily the dispersion data in Fig. 3(b) considering the same phonon dispersion for the four P_{ij} processes. The best fit was obtained when we considered different dispersions for the two iTO phonon branches of bilayer graphene. Table I shows the parameters obtained for each phonon branch, which exhibit a linear dispersion near the K point. Notice that the difference between these two phonon branches corresponds to a splitting of about 3 cm^{-1}, which is in close agreement with that reported previously.[6,9]

Table II shows the γ values obtained experimentally. The parameter γ_0, associated with the in-plane nearest neighbor

TABLE II. Experimental SWM parameters (in eV) for the band structure of bilayer graphene. The parameters for graphite are taken from Refs. 18 and 19.

	γ_0	γ_1	γ_2	γ_3	γ_4	γ_5	$\gamma_6=\Delta$
Bilayer graphene	2.9	0.30	n/a	0.10	0.12	n/a	n/a
Graphite	3.16	0.39	−0.02	0.315	0.044	0.038	0.008

hopping energy, is ten times larger than γ_1, which is associated with atoms from different layers along the vertical direction (see Fig. 1). These values are in good agreement with the previous angle resolved photoemission spectroscopy (ARPES) measurements in bilayer graphene.[17] The resolution of our experiment allows, however, the measurement of weaker hopping parameters (γ_3 and γ_4), that are beyond the current resolution of ARPES. The value of γ_1 is about three times larger than γ_3 and γ_4, both associated with the interlayer hopping not along the vertical direction (see Fig. 1).

The corresponding parameters found experimentally for graphite are also shown in Table II.[18,19] The parameters γ_0 and γ_1 for bilayer graphene are slightly smaller than those for graphite. This difference is more accentuated for the parameter γ_3. These results are in good agreement with the weak interlayer coupling parameters extracted from the first-principles calculations on the three dimensional graphite.[20,21] On the other hand, our value of γ_4 for bilayer graphene is significantly higher than the value for graphite measured by Mendez *et al.* in a magnetoreflection experiment.[22] Notice that this parameter is especially important since it is related to the difference of electron and hole effective masses in the valence and conduction bands.[19]

Finally, we must also comment that there are also other symmetry allowed weak terms which are not present in the standard SWM model. In particular, the next-nearest neighbor hopping process within each layer, denoted by t',[23] was already considered in the seminal paper by Wallace[15] and later on in the model reported by Johnson and Dresselhaus.[24] Similarly to the γ_4 parameter, t' also breaks the electron hole symmetry that is present in the simplest case considering only γ_0, γ_1, and γ_3. However, with the introduction of this new term in the least-square fitting process, we are faced with the problem of having too many fitting parameters, preventing an accurate determination of all parameters from the data. However, the important point is that the data shown in Fig. 3 cannot be explained without considering the asymmetry between electrons and holes.

In summary, from the resonant Raman study of the G' band of bilayer graphene using several laser excitation energies, we have been able to probe the dispersion of electrons and phonons of this material near the Dirac point. From the fitting of the experimental data using the SWM model, we have obtained experimental values for the interlayer hopping parameters for bilayer graphene, and the results reveal the asymmetry between the electronic dispersion curves in the valence and conduction bands. Finally, in a future work we will study DR processes involving holes, many-body effects,[25] as well as the biased bilayer graphene.

This work was supported by Rede Nacional de Pesquisa em Nanotubos de Carbono–MCT, Brasil and FAPEMIG. L.M.M., J.C.B, and D.C.E. acknowledge the support from the Brazilian Agency CNPq. We would like to thank Millie Dresselhaus and Ado Jorio for critical reading of the manuscript and for helpful discussions.

[1] A. K. Geim and K. S. Novoselov, Nat. Mater. **6**, 183 (2007).
[2] E. V. Castro, K. S. Novoselov, S. V. Morozov, N. M. R. Peres, J. M. B. Lopes dos Santos, J. Nilsson, F. Guinea, A. K. Geim, and A. H. Castro Neto, arXiv:cond-mat/0611342.
[3] J. B. Oostinga, H. B. Heersche, X. Liu, A. F. Morpurgo, and L. M. K. Vandersypen, arXiv:0707.2487.
[4] J. W. McClure, Phys. Rev. **108**, 612 (1957).
[5] J. C. Slonczewski and P. R. Weiss, Phys. Rev. **109**, 272 (1958).
[6] A. C. Ferrari, J. C. Meyer, V. Scardaci, C. Casiraghi, M. Lazzeri, F. Mauri, S. Piscanec, D. Jiang, K. S. Novoselov, S. Roth, and A. K. Geim, Phys. Rev. Lett. **97**, 187401 (2006).
[7] M. A. Pimenta, G. Dresselhaus, M. S. Dresselhaus, L. G. Cancado, A. Jorio, and R. Saito, Phys. Chem. Chem. Phys. **9**, 1276 (2007).
[8] A. Gupta, G. Chen, P. Joshi, S. Tadigadapa, and P. C. Eklund, Nano Lett. **6**, 2667 (2006).
[9] D. Graf, F. Molitor, K. Ensslin, C. Stampfer, A. Jungen, C. Hierold, and L. Wirtz, Nano Lett. **7**, 238 (2007).
[10] C. Thomsen and S. Reich, Phys. Rev. Lett. **85**, 5214 (2000).
[11] R. Saito, A. Jorio, A. G. Souza Filho, G. Dresselhaus, M. S. Dresselhaus, and M. A. Pimenta, Phys. Rev. Lett. **88**, 027401 (2001).
[12] J. Maultzsch, S. Reich, and C. Thomsen, Phys. Rev. B **70**, 155403 (2004).
[13] G. Ge. Samsonidze, Ph.D. thesis, Massachusetts Institute of Technology, 2007.
[14] E. McCann and V. I. Falko, Phys. Rev. Lett. **96**, 086805 (2006).
[15] P. R. Wallace, Phys. Rev. **71**, 622 (1947).
[16] B. Partoens and F. M. Peeters, Phys. Rev. B **74**, 075404 (2006).
[17] T. Ohta, A. Bostwick, J. L. McChesney, T. Seyller, K. Horn, and Eli Rotenberg, Phys. Rev. Lett. **98**, 206802 (2007).
[18] N. B. Brandt S. M. Chudinov, and Ya. G. Ponomarev, *Semimetals 1: Graphite and its Compounds* (North-Holland, Amsterdam, 1988).
[19] M. S. Dresselhaus, G. Dresselhaus, K. Sugihara, I. L. Spain, and H. A. Goldberg, *Carbon Fibers and Filaments* (Springer-Verlag, Berlin, Heidelberg, 1988), Chap. 7.
[20] R. C. Tatar and S. Rabii, Phys. Rev. B **25**, 4126 (1982).
[21] J.-C. Charlier, J.-P. Michenaud, and X. Gonze, Phys. Rev. B **46**, 4531 (1992).
[22] E. Mendez, A. Misu, and M. S. Dresselhaus, Phys. Rev. B **21**, 827 (1980).
[23] N. M. R. Peres, F. Guinea, and A. H. Castro Neto, Ann. Phys. (N.Y.) **321**, 1559 (2006).
[24] L. G. Johnson and G. Dresselhaus, Phys. Rev. B **7**, 2275 (1973).
[25] S. V. Kusminskiy, J. Nilsson, D. K. Campbell, and A. H. Castro Neto, arXiv:0706.2359.